Research Article | Vol. 28, No. 8 / 13 April 2020 / Optics Express 10888
Optics EXPRESS

Frequency-tuning dual-comb spectroscopy using silicon Mach-Zehnder modulators

LUCAS DENIEL,[1,*] ERWAN WECKENMANN,[2] DIEGO PÉREZ GALACHO,[1,3] CARLOS ALONSO-RAMOS,[1] FRÉDÉRIC BOEUF,[4] LAURENT VIVIEN,[1] AND DELPHINE MARRIS-MORINI[1]

[1] *Université Paris-Saclay, CNRS, Centre de Nanosciences et de Nanotechnologies, 91120 Palaiseau, France*
[2] *Univ Rennes, CNRS, FOTON - UMR 6082, F-22305 Lannion, France*
[3] *ITEAM Research Institute, Universitat Politècnica de València, Camino de Vera s/n, 46022 Valencia, Spain*
[4] *ST Microelectronics, 850 rue Jean Monnet, 38920 Crolles, France*
[*] *lucas.deniel@c2n.upsaclay.fr*

Abstract: Dual-comb spectroscopy using a silicon Mach-Zehnder modulator is reported for the first time. First, the properties of frequency combs generated by silicon modulators are assessed in terms of tunability, coherence, and number of lines. Then, taking advantage of the frequency agility of electro-optical frequency combs, a new technique for fine resolution absorption spectroscopy is proposed, named frequency-tuning dual-comb spectroscopy, which combines dual-comb spectroscopy and frequency spacing tunability to measure optical spectra with detection at a unique RF frequency. As a proof of concept, a 24 GHz optical bandwidth is scanned with a 1 GHz resolution.

1. Introduction

After revolutionizing optical frequency metrology and synthesis [1,2], optical frequency combs (OFCs) have found many novel applications in various fields including coherent and advanced format telecommunications [3–14], astronomy [15] or spectroscopy [16–31]. Commonly generated from lasers through mode-locking or non-linear optical processes [3,16–23,32], OFCs can also be produced through dissipative Kerr soliton generation in high quality factor microresonators (microcombs) [3,6–7,15–17,24–27,32–37], by parametric mixing [13], or by electro-optic modulation [3–4,8–12,16,28–31,38–53]. Frequency combs generated by electro-optic modulation, also called electro-optical frequency combs (EOFCs), offer the major advantage of being easily tunable, both in terms of central frequency, fixed by the input laser, and in line spacing (repetition rate), which is given by the frequency of the applied radio-frequency (RF) signal. As a comparison, the repetition rate of microcombs and laser-based combs are fixed by device design. Values of tens to hundreds of GHz are achieved for the microcombs [4,6–7,16–17,24–27,33–35], while the repetition rate of fiber laser-based combs are on the orders of tens or hundreds of MHz [3–4,16–17,19–22]. On the contrary, using EOFCs the repetition rate is fully tunable within the modulator electro-optic bandwidth, up to tens of GHz [3–4,8–12,16,28–31,38–52].

While OFCs could be exploited by spatially demultiplexing the generated comb teeth, the most attractive use of these devices is the multi-heterodyne or dual-comb configuration, which enables high frequency resolution and accuracy, within a fast detection technique, with many applications in spectroscopy and metrology [16–23,25–31,36–37,45–47,54–55]. By combining two combs with slightly different repetition rates on a photodetector, an image of the optical spectrum can be obtained by measuring the RF spectrum. The analysis of the optical spectrum thus relies on the measurement of the RF spectrum at the photodetector output. In this context, EOFCs present two key features: they provide frequency spacing tunability, and using the same laser source to

#390041 https://doi.org/10.1364/OE.390041
Journal © 2020 Received 12 Feb 2020; revised 23 Mar 2020; accepted 23 Mar 2020; published 30 Mar 2020

Optics EXPRESS

generate both combs enables a high mutual coherence time, avoiding the need for mutual comb locking.

In terms of photonics integration, Si photonics is a mature technology which benefits from high-volume fabrication. Low cost, small size, low weight systems are thus expected. High speed depletion-based silicon electro-optical modulators have shown robust performance in telecommunications for many years [56]. However the use of silicon modulator to generate EOFC is still sparse [10–12,41–45].

In this paper, the benefits of EOFC in terms of tunability are used to propose a new method for fine resolution absorption spectroscopy. Indeed dual-comb spectroscopy is combined with the agility to tune the frequency spacing of EOFCs to scan the optical spectrum while generating beat notes at fixed RF frequencies. The detection is then performed at fixed RF frequencies, allowing simple instrumentation. This is possible by tuning simultaneously the frequency spacing of both EOFCs, while keeping constant the difference between the two EOFCs frequency spacings. In the experimental demonstration, both EOFCs are generated on chip using a fixed wavelength laser source and two silicon-based Mach-Zehnder modulators (Si MZM). In the reported experiment, the mutual coherence between both combs is first investigated, showing a mutual coherence time better than 50 µs. The tunability of the EOFCs repetition rates is then studied between 1 and 12 GHz. Finally the proposed method is demonstrated by recovering the transfer function of an optical band-pass filter. Interestingly, using a fixed wavelength source and detecting two beat-notes, a 24 GHz optical bandwidth is scanned with a 1 GHz resolution.

2. Silicon MZM-based EOFC

2.1. Si modulator design, fabrication and performances

The Si modulator is a single-drive Mach-Zehnder modulator. The phase modulation is obtained by carrier depletion in PN diodes embedded in each arm of the Mach-Zehnder interferometer (MZI). Both PN junctions share the same electrical potential for the N side. The applied RF signal is thus distributed in opposite phases on the two arms, intrinsically setting the modulator in push-pull operation as illustrated in Fig. 1(b). The modulator was fabricated by STMicroelectronics, in their 300-mm SOI technological platform [57]. The waveguide width is 400 nm and its height is 300 nm, a slab thickness as low as 50 nm ensures a strong confinement of the guided mode, as shown in Fig. 1(a). Ion implantation is used to form the PN diode. Each phase shifter length is 4 mm. The modulator is working at a wavelength of 1.55 µm, with a 3 dB optical bandwidth of 35 nm, essentially limited by the grating couplers. Metallic resistive strip lines are placed above each arm as heaters to tune the static phase difference between the two arms by thermo-optic effect, under the application of a small DC voltage.

The measured V_π is 8 V and an 18 GHz small-signal electro-optic bandwidth was measured using a Lightwave component analyzer. Optical losses due to free carrier absorption have been estimated by numerical simulation. A value of 1.24 dB×mm^{-1} is obtained at 0 V, decreasing to 0.63 dB×mm^{-1} at -14 V.

2.2. Heterodyne detection of frequency combs from Si EOFC generator

The principle of electro-optic comb generation lies in the nonlinearity of the electro-optical modulation [Fig. 2(a)]. By undergoing a sinusoidal phase modulation (frequency f_{REP}), the optical carrier alternatively experiences positive and negative chirps. The instantaneous frequency of the electric field is thus periodically oscillating at the repetition rate f_{REP}. The corresponding spectrum therefore contains a set of discrete frequency lines, separated by the modulation frequency [43]. Indeed, if we consider an electric field E_{IN} at the input of a phase modulator,

Optics EXPRESS

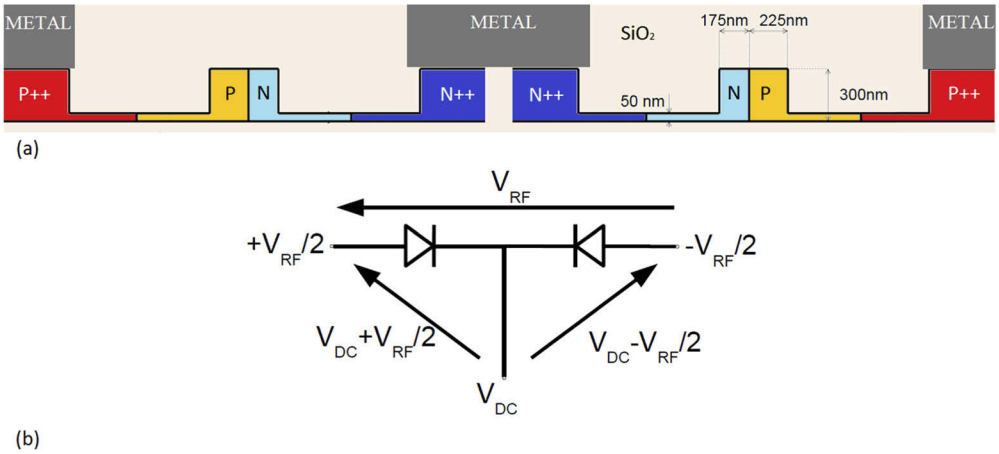

Fig. 1. (a) Cut view of the waveguide phase shifter. (b) The Si modulator equivalent electrical scheme and driving configuration.

oscillating at the angular frequency ω_0, it can be expressed as:

$$E_{IN} = E_0 \times \exp(\mathrm{j}\omega_0 \mathrm{t}) \tag{1}$$

After undergoing phase modulation, the field at the output becomes:

$$E_{OUT} = E_{IN} \times \exp(j[A \times \sin(\omega_{\mathrm{REP}} \mathrm{t})]) \tag{2}$$

where A is the phase modulation amplitude, and $\omega_{\mathrm{REP}} = 2\pi \times \mathrm{f}_{\mathrm{REP}}$ is the angular frequency of the modulation. According to the Jacobi-Anger expansion, Eq. (2) can be written as:

$$E_{OUT} = E_{IN} \times \sum_{n=-\infty}^{\infty} J_n(A) \exp(j[n \times \omega_{REP} \mathrm{t}]) \tag{3}$$

where $\mathrm{J_n}()$ is the $\mathrm{n^{th}}$ order Bessel function of the first kind. As it can be seen from this expression, new lines are generated at angular frequencies ($\omega_0 + \mathrm{n} \times \omega_{\mathrm{REP}}$), and the nth order line is weighed by a coefficient $\mathrm{J_n(A)}$. When the electric field $\mathrm{E_{OUT,1}}$ at the output of the first MZM arm is combined with the electric field $\mathrm{E_{OUT,2}}$ at the output the second MZM arm, with a heater phase offset φ_{H}, the total electric field exiting the modulator is:

$$E_{TOT} = \frac{E_{OUT,1} + E_{OUT,2} \times \exp(\mathrm{j}\varphi_H)}{\sqrt{2}} \tag{4}$$

In plasma dispersion effect-based silicon phase modulators, an amplitude modulation of the electric field occurs along with phase modulation, which makes the Jacobi-Anger expansion formalism unsuitable in this situation. A numerical model of the MZM is therefore implemented to simulate the Si EOFC generator. Both the effective index and the optical loss due to free carrier concentration variation with applied voltage are considered in the modeling of phase shifters. After using Eq. (4) to combine the modulated output of each MZM arm, a fast Fourier transform algorithm converts the temporal evolution of the field into the optical spectrum. Figure 2(b) shows the simulated spectrum, for a 22 dBm-RF signal at 2 GHz frequency. A set of frequency lines separated by $\mathrm{f_{REP}}$ is obtained. The amplitude of the different lines, i.e. the achieved spectrum shape depends on the static optical phase difference between both arms of the MZM. Each comb line is labeled by its frequency $\mathrm{f_n}$, n being a line number, the carrier is $\mathrm{f_0}$.

Optics EXPRESS

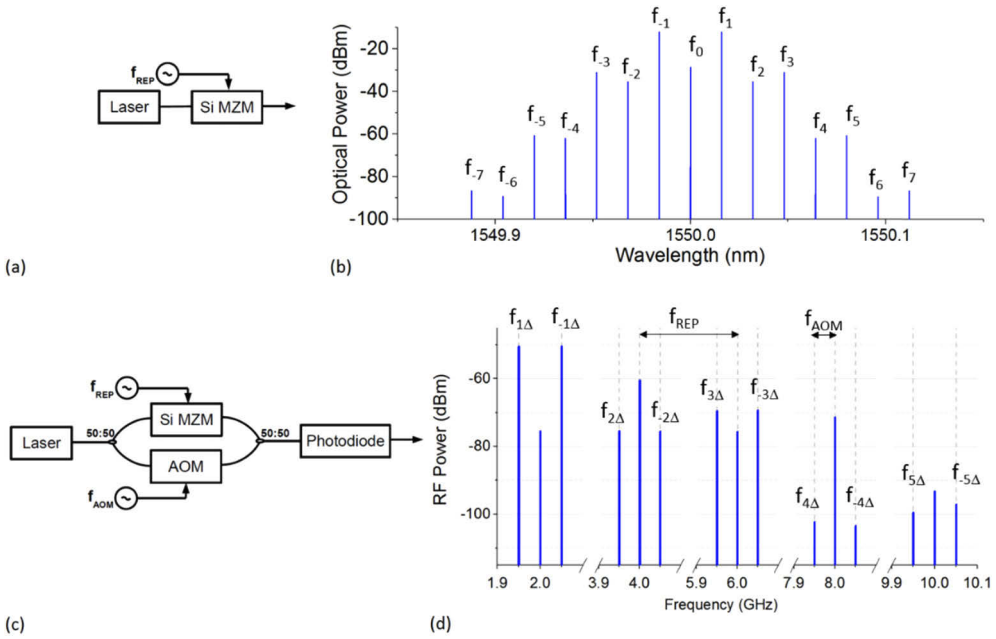

Fig. 2. (a) Generic schematic for EOFC generation, Si MZM: silicon Mach-Zehnder modulator. (b) Example of a simulated Si EOFC spectrum. The repetition rate (f_{REP}) is 2 GHz and the laser wavelength is 1550 nm. The MZM is biased with a $1.1\times\pi$ phase difference between both arms. Each line is labeled by its frequency f_n, with n being the line number; the carrier frequency is f_0. (c) Generic schematic for heterodyne detection of an EOFC. AOM: acousto-optic modulator. (d) Simulated heterodyne detection of a Si EOFC. The applied RF power is 24 dBm, the acousto-optic frequency (f_{AOM}) is 40 MHz. A zoom near the successive beatings at $n \times f_{REP}$ provides an image of the optical comb in the RF domain. The beating between each optical line f_n and the shifted laser line is labeled with its frequency $f_{n\Delta}=|f_n-(f_0+f_{AOM})|$.

As standard grating-based optical spectrum analyzers do not provide enough resolution to resolve the individual lines of an EOFC with a line spacing of a few GHz, a heterodyne technique can be used to map the optical comb in the RF domain. This method is schematically illustrated in Fig. 2(c). The laser output is separated in two beams, one that is sent to the Si MZM to generate the optical comb, while the frequency of the second beam is shifted using an acousto-optic modulator. The shifted line acts as a local oscillator when mixed with the comb in a photodiode. The resulting electrical spectrum thus contains an image of the optical comb, folded on itself by its beating with the shifted laser-line. Such heterodyne detection technique has been modeled, and the electrical spectrum obtained from the simulation can be seen in Fig. 2(d). It can be observed that the resulting spectrum is a set of groups of 3 lines, repeated around the multiples of the comb repetition frequency (2 GHz for the considered frequency). In each set of 3 lines, the right and left lines ($f_{n\Delta}$) are images of the EOFC lines f_n [Fig. 2(b)], beating with the local oscillator whose optical frequency is f_0+f_{AOM}. Finally, the middle line in each set corresponds to multiple beatings between EOFC lines themselves.

The set-up in Fig. 2(c) was used to measure EOFCs generated by a Si modulator. For all the experiments, the PN junctions are reverse biased by a -6 V DC voltage. A 22 dBm (peak to peak voltage of 8 Volts) sinusoidal RF signal at 2 GHz is applied to the modulator, and a 40 MHz sinusoidal signal is applied to the acousto-optic modulator to shift the laser line. The laser wavelength is set to 1.55 μm and the total optical power received on the photodiode is 0

Optics EXPRESS

dBm. The photodiode is connected to an electrical spectrum analyzer (ESA), with a resolution bandwidth of 100kHz. The measured spectrum is shown in Fig. 3. A total of 11 EOFC lines were recovered (the beating between the carrier and the local oscillator at 40 MHz is not shown in Fig. 3), in good agreement with those obtained by simulation [Fig. 2(d)]. Similar experiments were performed, with Si modulator driving frequencies of 1, 3, and 5 GHz, showing equivalent performance.

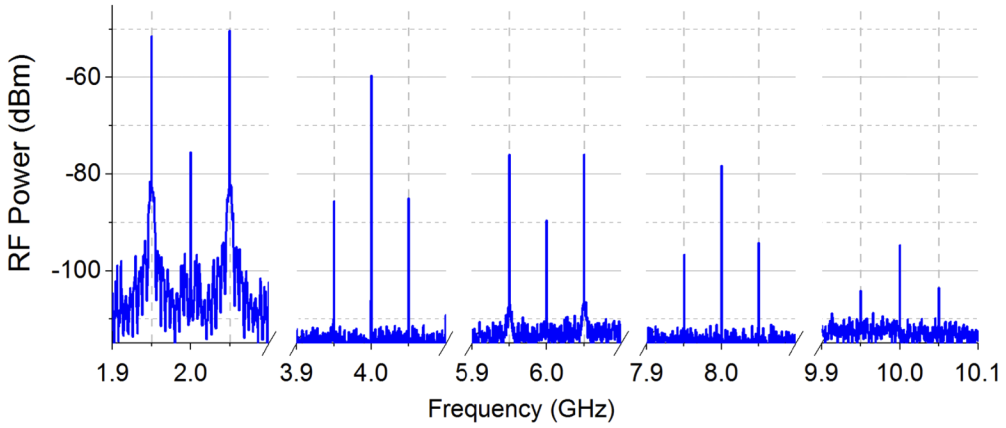

Fig. 3. Experimentally measured heterodyne beating of the Si EOFC with a laser line shifted by 40 MHz from the comb center.

3. Dual-comb spectroscopy using Si EOFC generators

Dual-comb spectroscopy is a well-known technique that enables high frequency resolution measurements. It relies on the beating of two OFCs with slightly different frequency spacings ($f_{REP,1}$ and $f_{REP,2} = f_{REP,1} + \Delta f_{REP}$). Each pair of comb lines creates a beat note at a frequency given by the separation between the comb lines. Thus it is possible to map the optical spectrum to an RF spectrum, with a resolution of about $f_{REP,1}$ while the spectral width is stretched by a factor $\Delta f_{REP} / f_{REP}$. If one or both OFC pass through a substance to be detected it is possible to recover its transmission spectra, by the measurement of the beat notes in the RF domain. Interestingly, by ensuring a high mutual coherence between the two OFCs, the dual-comb interferogram can be recorded over a long period of time, and the resulting high amount of collected optical power provides an improved signal-to-noise ratio [16–20,22,26–27,53]. On the other side, real-time measurement can also be performed, enabling direct observations of transient responses of complex optical spectra [16–18,26–27,37,47]. In both cases, EOFC is a well suited solution for dual-comb spectroscopy: since a single laser can be used to generate the two EOFCs, a high mutual coherence is naturally ensured between them, avoiding the need to lock one comb to the other, and the flexibility of EOFCs allows to tune straightforwardly the combs frequency spacings [3–4,16,28–31,47].

In the experimental demonstration, the two EOFCs are generated on a chip using single drive Si MZMs. Coherence properties and repetition rate tuning of Si-based EOFCs in dual-comb configuration are evaluated using the experimental set-up represented in Fig. 4(a). To avoid aliasing in the measured beat notes, an acousto-optic modulator (AOM) is used to shift one OFC in frequency by 40 MHz. The two combs are then combined and sent to a 32 GHz-photodiode, followed by an electrical spectrum analyzer.

The two RF synthesizers deliver a 24 dBm signal and are synchronized with a 10 MHz reference. Figure 4(b) presents the measured beat notes, for $f_{AOM} = 40$ MHz, $f_{REP,1} = 500$ MHz

Optics EXPRESS

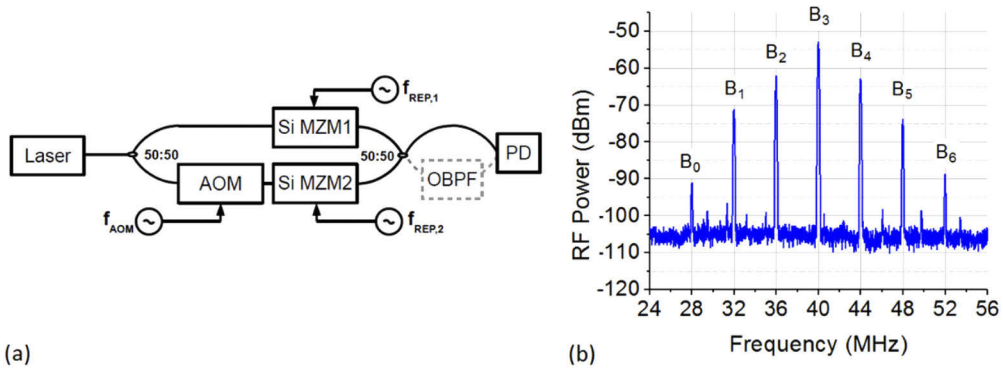

Fig. 4. (a) Experimental setup for the dual Si-EOFC generation and measurement. Si MZM: silicon Mach-Zehnder modulator, AOM: acousto-optic modulator, PD: photodiode, OBPF: optical band-pass filter, used to illustrate the proposed scanning method: the transfer function of the OBPF will be recovered by the dual EOFC measurement. (b) Example of a dual Si-EOFC beat signal measured experimentally for a repetition rate ($f_{REP,1}$) of 500 MHz, a repetition rate offset (Δf_{REP}) of 4 MHz, using 24 dBm RF power on each synthetizer, and an acousto-optic frequency (f_{AOM}) of 40 MHz. Each beat note is identified by a capital letter B and an index number. B_3 corresponds to the beating between the two EOFC central lines.

and $f_{REP,2} = 504$ MHz. 7 lines separated by 4 MHz emerge from the measurement noise floor while the ESA resolution bandwidth is set to 100 kHz. The reduction of the number of lines in the dual-comb experiment in comparison with the characterization of single EOFC is explained by the lower power of the higher order frequency lines of the two EOFC that are combined. Indeed when the power levels of two optical lines are decreased by a factor α, the corresponding photodetected beat note electrical power decreases by a factor α^2.

To assess the coherence properties of the Si-based EOFCs, a zoomed superposition of the different beat notes is reported in Fig. 5(a), the resolution bandwidth of the ESA is set to 10 kHz for this measurement. Interestingly their 3 dB linewidth is below 20 kHz, which corresponds to a mutual coherence time better than 50 µs [26].

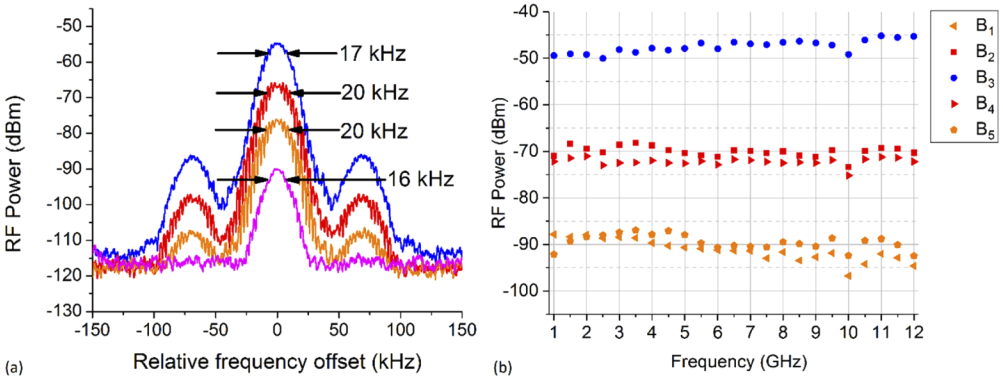

Fig. 5. (a) Superposed beat notes B_3 to B_6, around their relative frequencies. (b) Power of the B_1 to B_5 beat-notes for applied frequencies of 1 GHz to 12 GHz.

To confirm the simple tuning of Si-based EOFCs, their frequency spacings have been tuned by adjusting $f_{REP,1}$ and $f_{REP,2}$, while Δf_{REP} is kept constant and equal to 4 MHz. In Fig. 5(b), the RF power levels of the 5 main beat notes are shown, when $f_{REP,1}$ is swept from 1 to 12 GHz. The

Optics EXPRESS

RF power applied on each modulator is 24 dBm. It can be seen that the power of all beat notes remains steady over this frequency range, and the effect of the modulator bandwidth is barely noticeable.

4. Frequency tuning dual-comb spectroscopy (FT-DCS): proof of concept

Frequency-tuning dual-comb spectroscopy (FT-DCS) is proposed for fine resolution spectroscopy using detection at fixed RF frequencies. Thus it would be possible to use electronic band-pass filters and amplifiers to extract the power of individual lines without affecting the system flexibility. This method relies on the extremely easy tuning of the frequency spacing of EOFCs to measure optical spectra with a high precision.

In the FT-DCS, both EOFCs frequency spacing ($f_{REP,1}$ and $f_{REP,2} = f_{REP,1} + \Delta f_{REP}$) are tuned simultaneously to cover the optical spectrum around the laser frequency, while Δf_{REP} is kept constant. Thus, by measuring the power of the fundamental beat notes at frequencies $f_{AOM} + \Delta f_{REP}$ and/or $f_{AOM} - \Delta f_{REP}$ for the different values of $f_{REP,1}$, it is possible to image the entire optical spectrum.

As a proof of concept, an optical band-pass filter (YENISTA XTM-50) was placed just before the photodiode [i.e. the output of the combiner is switched to the grey dashed path in Fig. 4(a)]. To recover the transfer function of this filter, the powers of the fundamental beat notes [i.e. B2 and B4 in Fig. 4(b)] were measured for different repetition rates ($f_{REP,1}$ was swept manually from 0.5 GHz to 12.5 GHz), while the repetition rate difference between the two EOFCs was kept constant ($\Delta f_{REP} = 4$ MHz). A reference dual-comb spectrum was also taken at each step by bypassing the filter. It is then possible to reconstruct the optical spectrum by subtraction and normalization of the two measurements.

Figure 6(a) shows the optical transfer function of the filter, recovered by the Si-based FT-DCS method (red points). The grey dashed line indicates the measurement noise floor, given by the difference between the fundamental beat note power of the reference dual-comb spectrum and the ESA noise floor, while the resolution bandwidth is 100 kHz. The resulting optical signal-to-noise ratio (OSNR) is about 15 dB. An alternative measurement of the filter transfer function was later performed using a YENISTA CT400 component tester. By direct sweeping the tunable laser over the 25 GHz span, with a 125 MHz step, the optical transmission was recorded at

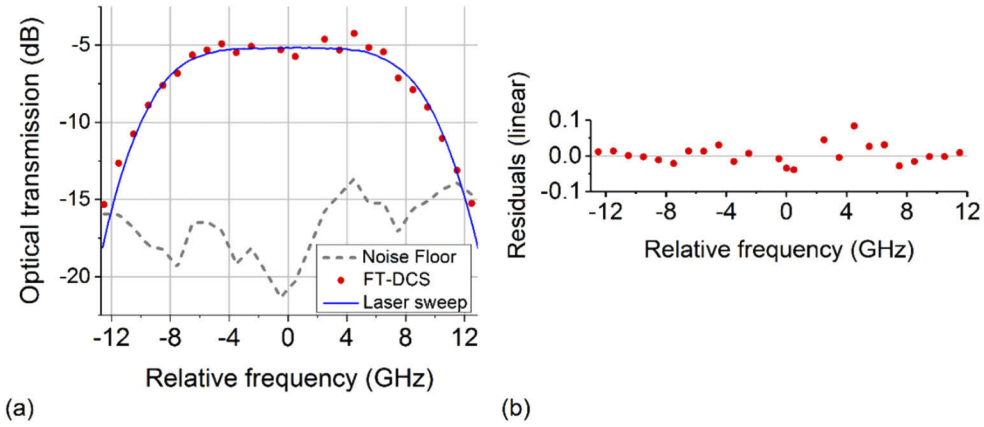

Fig. 6. (a) Optical transfer function of an optical filter, recovered by FT-DCS (red points), laser sweep (blue curve), the grey dashed line is the optical noise floor of the dual-comb scanning method. (b) The residuals from the dual-comb scanning method, compared to the sweep laser measurement, show a 2.69% standard deviation.

Optics EXPRESS

each step, resulting in the blue curve in Fig. 6(a). Due to a ±5 GHz uncertainty on the tunable external cavity laser output absolute frequency, the two measurements initially showed a static 4.75 GHz mismatch. To reduce this static mismatch, a referenced laser with higher frequency accuracy has to be used [29,52]. However to compare the shape of the recover filter spectra, both measurements have thus been normalized in frequency, relatively to the filter transfer function center. When comparing both measurements, a very good agreement is seen. A 10 dB bandwidth of 24 GHz (0.19 nm) is obtained in both cases. The difference between both measurements is displayed in a linear scale as residuals in Fig. 6(b), and the standard deviation is estimated to be 2.7%, confirming the very good precision of the FT-DCS method for spectral measurements.

5. Discussion

In this work the FT-DCS has been proposed as a fine resolution spectroscopy technique, and only two beat notes (b_2 and b_4) were measured while scanning the spectrum. However, Si-based EOFC generators can also be used in more classical dual-comb spectroscopy experiments where a large number of flat lines are usually required. In this case the performances in terms of spectral spanning are given by the modulator electro-optic bandwidth, which gives the maximum line spacing, and by the modulation efficiency which gives the maximum number of lines above a given power threshold. Optimizing simultaneously those parameters to map a wide spectral range using a single modulator usually leads to a tradeoff as, when increasing the phase shifter length to optimize the phase modulation efficiency, the electro-optic bandwidth is then limited by RF signal propagation loss, and by the mismatch between the optical and electrical propagating velocities. This tradeoff has been studied already in $LiNbO_3$ modulators, and the results can be translated to Si modulators. Among the possible solutions to optimize the EOFC performances it is possible: (i) to cascade several modulators and/or to cascade amplitude and phase modulation, to flatten the frequency comb as shown in [4,58]; (ii) to use electrical signals containing two or more frequencies to drive each modulator [41]; (iii) to use a resonant cavity, so that when the modulation frequency meets the cavity free spectral range, the light is being constructively modulated at each round trip, which is also equivalent to an increase of the effective modulator length [40]. All of these solutions could be implemented in Si photonics, for the generation of flat, frequency tunable and wide bandwidth frequency combs. Furthermore it can be added that the external AOM used in the experiment can also be replaced by an on-chip frequency shifter, such as a dual-parallel IQ modulator also achievable within Si photonics platform.

6. Conclusion

Dual-comb spectroscopy using silicon single-drive push-pull MZMs is reported for the first time. The general properties of Si-based EOFCs (tunability, coherence, number of lines) have been assessed. Then, taking benefit of the frequency agility of EOFCs, we proposed a new technique for fine resolution spectroscopy within a simple experimental set-up. This method, named frequency-tuning dual-comb spectroscopy (FT-DCS), relies on the extremely easy tuning of the frequency spacing of EOFCs to measure optical spectra with a high precision, using a single-wavelength laser and a simple detection at a unique RF frequency. By sweeping the repetition rate of the two EOFCs within the modulator bandwidth, and keeping their frequency spacing difference constant, the measurement of the fundamental beat notes allows to scan the optical spectrum and to measure sample absorption. As a proof of concept, the amplitude transfer function of an optical filter has been measured. The 10 dB-bandwidth of 24 GHz (0.19 nm) was retrieved, and the transfer function was successfully compared with classical tunable laser experiment. These results pave the way for further absorption spectroscopy applications as the achievable frequency range are compatible with typical molecules absorption linewidth. Furthermore, the use of silicon photonics, as a mature technology platform which benefits

Optics EXPRESS

from CMOS fabrication facilities opens the path towards large scale fabrication of compact spectroscopic systems.

Funding

Agence Nationale de la Recherche (ANR-17-CE09-0041, ANR-18-CE39-0009).

Acknowledgments

Diego Perez-Galacho acknowledges the support of the Spanish Ministry of Science, Innovation and Universities through the Juan de la Cierva fellowship program.

Disclosures

The authors declare no conflicts of interest.

References

1. S. A. Diddams, D. J. Jones, L. S. Ma, S. T. Cundiff, and J. L. Hall, "Optical frequency measurement across a 104-THz gap with a femtosecond laser frequency comb," Opt. Lett. **25**(3), 186–188 (2000).
2. S. T. Cundiff, J. Ye, and J. L. Hall, "Optical frequency synthesis based on mode-locked lasers," Rev. Sci. Instrum. **72**(10), 3749–3771 (2001).
3. V. Torres-Company, J. Schröder, A. Fülöp, M. Mazur, L. Lundberg, Ó. B. Helgason, M. Karlsson, and P. A. Andrekson, "Laser Frequency Combs for Coherent Optical Communication," J. Lightwave Technol. **37**(7), 1663–1670 (2019).
4. V. Torres-Company and A. M. Weiner, "Optical frequency comb technology for ultra-broadband radio-frequency photonics," Laser Photonics Rev. **8**(3), 368–393 (2014).
5. S. T. Cundiff and A. M. Weiner, "Optical arbitrary waveform generation," Nat. Photonics **4**(11), 760–766 (2010).
6. A. Fülöp, M. Mazur, A. Lorences-Riesgo, T. A. Eriksson, P. Wang, Y. Xuan, D. E. Leaird, M. Qi, P. A. Andrekson, A. M. Weiner, and V. Torres-Company, "Long-haul coherent communications using microresonator-based frequency combs," Opt. Express **25**(22), 26678–26688 (2017).
7. P. Marin-Palomo, J. N. Kemal, M. Karpov, A. Kordts, J. Pfeifle, M. H. P. Pfeiffer, P. Trocha, S. Wolf, V. Brasch, M. H. Anderson, R. Rosenberger, K. Vijayan, W. Freude, T. J. Kippenberg, and C. Koos, "Microresonator-based solitons for massively parallel coherent optical communications," Nature **546**(7657), 274–279 (2017).
8. C. Weimann, P. C. Schindler, R. Palmer, S. Wolf, D. Bekele, D. Korn, J. Pfeifle, S. Koeber, R. Schmogrow, L. Alloatti, D. Elder, H. Yu, W. Bogaerts, L. R. Dalton, W. Freude, J. Leuthold, and C. Koos, "Silicon-organic hybrid (SOH) frequency comb sources for terabit/s data transmission," Opt. Express **22**(3), 3629–3637 (2014).
9. N. Dupuis, C. R. Doerr, L. Zhang, L. Chen, N. J. Sauer, P. Dong, L. L. Buhl, and D. Ahn, "InP-Based Comb Generator for Optical OFDM," J. Lightwave Technol. **30**(4), 466–472 (2012).
10. J. Lin, H. Sepehrian, Y. Xu, L. A. Rusch, and W. Shi, "Frequency Comb Generation using a CMOS Compatible SiP DD-MZM for Flexible Networks," IEEE Photonics Technol. Lett. **30**(17), 1495–1498 (2018).
11. X. Xiao, M. Li, L. Wang, D. Chen, Q. Yang, and S. Yu, "High speed silicon photonic modulators," *In Optical Fiber Communications Conference and Exhibition (OFC)*, Los Angeles, CA, USA, March 19-23, 2017; IEEE, 2017, pp. 1–3 (2017).
12. Y. Xu, J. Lin, R. Dubé-Demers, S. LaRochelle, L. Rusch, and W. Shi, "Integrated flexible-grid WDM transmitter using an optical frequency comb in microring modulators," Opt. Lett. **43**(7), 1554–1557 (2018).
13. B. Ping-Piu Kuo, E. Myslivets, V. Ataie, E. G. Temprana, N. Alic, and S. Radic, "Wideband parametric frequency comb as coherent optical carrier," J. Lightwave Technol. **31**(21), 3414–3419 (2013).
14. J. Qian, S. Tian, and L. Shang, "Investigation on Nyquist pulse generation by optical frequency," J. Opt. Technol. **83**(11), 699–702 (2016).
15. E. Obrzud, M. Rainer, A. Harutyunyan, M. H. Anderson, J. Liu, M. Geiselmann, B. Chazelas, S. Kundermann, S. Lecomte, M. Cecconi, A. Ghedina, E. Molinari, F. Pepe, F. Wildi, F. Bouchy, T. J. Kippenberg, and T. Herr, "A microphotonic astrocomb," Nat. Photonics **13**(1), 31–35 (2019).
16. N. Picqué and T. W. Hänsch, "Frequency comb spectroscopy," Nat. Photonics **13**(3), 146–157 (2019).
17. G. Scalari, J. Faist, and N. Picqué, "On-chip mid-infrared and THz frequency combs for spectroscopy," Appl. Phys. Lett. **114**(15), 150401 (2019).
18. I. Coddington, N. R. Newbury, and W. C. Swann, "Dual-comb spectroscopy," Optica **3**(4), 414–426 (2016).
19. Z. Chen, M. Yan, T. W. Hänsch, and N. Picqué, "A phase-stable dual-comb interferometer," Nat. Commun. **9**(1), 3035 (2018).
20. I. Coddington, W. C. Swann, and N. R. Newbury, "Coherent Multiheterodyne Spectroscopy Using Stabilized Optical Frequency Combs," Phys. Rev. Lett. **100**(1), 013902 (2008).
21. S. Okubo, K. Iwakuni, H. Inaba, K. Hosaka, A. Onae, H. Sasada, and F. Hong, "Ultra-broadband dual-comb spectroscopy across 1.0–1.9 μm," Appl. Phys. Express **8**(8), 082402 (2015).

Optics EXPRESS

22. N. B. Hébert, J. Genest, J. Deschênes, H. Bergeron, G. Y. Chen, C. Khurmi, and D. G. Lancaster, "Self-corrected chip-based dual-comb spectrometer," Opt. Express **25**(7), 8168–8179 (2017).
23. G. Villares, A. Hugi, S. Blaser, and J. Faist, "Dual-comb spectroscopy based on quantum-cascade-laser frequency combs," Nat. Commun. **5**(1), 5192 (2014).
24. M. Yu, Y. Okawachi, C. Joshi, X. Ji, M. Lipson, and A. L. Gaeta, "Gas-Phase Microresonator-Based Comb Spectroscopy without an External Pump Laser," ACS Photonics **5**(7), 2780–2785 (2018).
25. M. Suh, Q. Yang, K. Y. Yang, X. Yi, and K. J. Vahala, "Microresonator soliton dual-comb spectroscopy," Science **354**(6312), 600–603 (2016).
26. A. Dutt, C. Joshi, X. Ji, J. Cardenas, Y. Okawachi, K. Luke, A. L. Gaeta, and M. Lipson, "On-chip dual-comb source for spectroscopy," Sci. Adv. **4**(3), e1701858 (2018).
27. M. Yu, Y. Okawachi, A. G. Griffith, N. Picqué, M. Lipson, and A. L. Gaeta, "Silicon-chip-based mid-infrared dual-comb spectroscopy," Nat. Commun. **9**(1), 1869 (2018).
28. G. Millot, S. Pitois, M. Yan, T. Hovhannisyan, A. Bendahmane, T. W. Hänsch, and N. Picqué, "Frequency-agile dual-comb spectroscopy," Nat. Photonics **10**(1), 27–30 (2016).
29. A. J. Fleisher, D. A. Long, J. T. Hodges, and D. F. Plusquellic, "Multiheterodyne Infrared Spectroscopy with Pitch-agile Optical Frequency Comb Generators," *In Fourier Transform Spectroscopy and Hyperspectral Imaging and Sounding of the Environment, Lake Arrowhead*, USA, March 1-4, 2015; OSA Technical Digest, FT2A.2 (2015).
30. D. A. Long, A. J. Fleisher, K. O. Douglass, D. E. Maxwell, K. Bielska, J. T. Hodges, and D. F. Plusquellic, "Multiheterodyne spectroscopy with optical frequency combs generated from a continuous-wave laser," Opt. Lett. **39**(9), 2688–2690 (2014).
31. A. Shams-Ansari, M. Yu, Z. Chen, C. Reimer, M. Zhang, N. Picqué, and M. Loncar, "Microring Electro-optic Frequency Comb Sources for Dual-Comb Spectroscopy," *In Conference on Lasers and Electro-Optics (CLEO)*, San Jose, USA, May 5-10, 2019; OSA Technical Digest, JTh5B.8 (2019).
32. A. L. Gaeta, M. Lipson, and T. J. Kippenberg, "Photonic-chip-based frequency combs," Nat. Photonics **13**(3), 158–169 (2019).
33. T. J. Kippenberg, A. L. Gaeta, M. Lipson, and M. L. Gorodetsky, "Dissipative Kerr solitons in optical microresonators," Science **361**(6402), eaan8083 (2018).
34. T. Tanabe, S. Fujii, and R. Suzuki, "Review on microresonator frequency combs," Jpn. J. Appl. Phys. **58**(SJ), SJ0801 (2019).
35. C. Wang, M. Zhang, M. Yu, R. Zhu, H. Hu, and M. Loncar, "Monolithic lithium niobate photonic circuits for Kerr frequency comb generation and modulation," Nat. Commun. **10**(1), 978 (2019).
36. N. G. Pavlov, G. Lihachev, S. Koptyaev, E. Lucas, M. Karpov, N. M. Kondratiev, I. A. Bilenko, T. J. Kippenberg, and M. L. Gorodetsky, "Soliton dual frequency combs in crystalline microresonators," Opt. Lett. **42**(3), 514–517 (2017).
37. C. Bao, M. Suh, and K. Vahala, "Microresonator soliton dual-comb imaging," Optica **6**(9), 1110–1116 (2019).
38. N. Yokota and H. Yasaka, "Operation strategy of InP Mach–Zehnder modulators for flat optical frequency comb generation," IEEE J. Quantum Electron. **52**(8), 1–7 (2016).
39. T. Ren, M. Zhang, C. Wang, L. Shao, C. Reimer, Y. Zhang, O. King, R. Esman, T. Cullen, and M. Loncar, "An Integrated Low-Voltage Broadband Lithium Niobate Phase Modulator," IEEE Photonics Technol. Lett. **31**(11), 889–892 (2019).
40. M. Zhang, B. Buscaino, C. Wang, A. Shams-Ansari, C. Reimer, R. Zhu, J. M. Kahn, and M. Lončar, "Broadband electro-optic frequency comb generation in a lithium niobate microring resonator," Nature **568**(7752), 373–377 (2019).
41. Z. Wang, M. Ma, H. Sun, M. Khalil, R. Adams, K. Yim, X. Jin, and L. R. Chen, "Optical frequency comb generation using CMOS compatible cascaded Mach–Zehnder modulators," IEEE J. Quantum Electron. **55**(6), 1–6 (2019).
42. I. Demirtzioglou, C. Lacava, K. R. H. Bottrill, D. J. Thomson, G. T. Reed, D. J. Richardson, and P. Petropoulos, "Frequency comb generation in a silicon ring resonator modulator," Opt. Express **26**(2), 790–796 (2018).
43. K. P. Nagarjun, V. Jeyaselvan, S. K. Selvaraja, and V. R. Supradeepa, "Generation of tunable, high repetition rate optical frequency combs using on-chip silicon modulators," Opt. Express **26**(8), 10744–10753 (2018).
44. X Wu and H. K. Tsang, "Flat-top Frequency Comb Generation with Silicon Microring Modulator and Filter," *In Conference on Lasers and Electro-Optics (CLEO)*, San Jose, USA, May 14-19, 2017; OSA Technical Digest, SM4O.6 (2017).
45. C. Weimann, M. Lauermann, F. Hoeller, W. Freude, and C. Koos, "Silicon photonic integrated circuit for fast and precise dual-comb distance metrology," Opt. Express **25**(24), 30091–30104 (2017).
46. E. L. Teleanu, V. Durán, and V. Torres-Company, "Electro-optic dual-comb interferometer for high-speed vibrometry," Opt. Express **25**(14), 16427–16436 (2017).
47. E. L. Teleanu, S. Tainta, and V. Torres-Company, "Ultrafast electrooptic dual-comb interferometry," Opt. Express **23**(23), 30557–30569 (2015).
48. T. Sakamoto, T. Kawanishi, and M. Tsuchiya, "10 GHz, 24 ps pulse generation using a single-stage dual-drive Mach-Zehnder modulator," Opt. Lett. **33**(8), 890–892 (2008).
49. R. Wu, V. R. Supradeepa, C. M. Long, D. E. Leaird, and A. M. Weiner, "Generation of very flat optical frequency combs from continuous-wave lasers using cascaded intensity and phase modulators driven by tailored radio frequency waveforms," Opt. Lett. **35**(19), 3234–3236 (2010).

Optics EXPRESS

50. A. J. Metcalf, V. Torres-Company, D. E. Leaird, and A. M. Weiner, "High-Power Broadly Tunable Electrooptic Frequency Comb Generator," IEEE J. Sel. Top. Quantum Electron. **19**(6), 231–236 (2013).
51. H. Kim, A. J. Metcalf, O. E. Sandoval, D. E. Leaird, and A. M. Weiner, "Broadband and ultra-flat optical comb generation using an EO comb source and a programmable pulse shaper," *In Conference on Lasers and Electro-Optics (CLEO) - Laser Science to Photonic Applications*, San Jose, USA, June 8-13, 2014; IEEE, pp. 1–2 (2014).
52. K. Beha, D. C. Cole, P. Del'Haye, A. Coillet, S. A. Diddams, and S. B. Papp, "Electronic synthesis of light," Optica **4**(4), 406–411 (2017).
53. P. Martín-Mateos, B. Jerez, P. Largo-Izquierdo, and P. Acedo, "Frequency accurate coherent electro-optic dual-comb spectroscopy in real-time," Opt. Express **26**(8), 9700–9713 (2018).
54. Z. Zhu and G. Wu, "Dual-Comb Ranging," Engineering **4**(6), 772–778 (2018).
55. M. Gianella, A. Nataraj, B. Tuzson, P. Jouy, F. Kapsalidis, M. Beck, M. Mangold, A. Hugi, J. Faist, and L. Emmenegger, "High-resolution and gapless dual comb spectroscopy with current-tuned quantum cascade lasers," Opt. Express **28**(5), 6197–6208 (2020).
56. W. Shi, Y. Xu, H. Sepehrian, S. LaRochelle, and L. A. Rusch, "Silicon photonic modulators for PAM transmissions," J. Opt. **20**(8), 083002 (2018).
57. C. Baudot, A. Fincato, D. Fowler, D. Perez-Galacho, A. Souhaité, S. Messaoudène, R. Blanc, C. Richard, J. Planchot, C. De-Buttet, B. Orlando, F. Gays, C. Mezzomo, B. Bernard, D. Marris-Morini, L. Vivien, C. Kopp, and F. Boeuf, "Daphne silicon photonics technological platform for research and development on WDM applications," Proc. SPIE **9891**, 98911D (2016).
58. V. Torres-Company, J. Lancis, and P. Andrés, "Lossless equalization of frequency combs," Opt. Lett. **33**(16), 1822–1824 (2008).